Journal of Power Sources, 27 (1989) 273 - 286

ELECTRO-OXIDATION MECHANISM OF GLYOXAL ON A GOLD ELECTRODE IN ACIDIC MEDIA

J. GONZÁLEZ-VELASCO

Departamento de Química — Facultad de Ciencias, Universidad Autónoma de Madrid, 28049 Madrid (Spain)

(Received August 5, 1988; in revised form May 18, 1989)

Summary

The electro-oxidation mechanism of glyoxal on a polycrystalline gold electrode in acidic solution has been studied. The oxidation takes place in the potential range at which OH and oxide coverages are formed and proceeds via a sequence of chemical and electro-chemical steps with the formation of oxalic acid and finally CO_2 and water. The kinetic parameters measured allow the formulation of a mechanism in which the formation of OH coverage and glyoxal adsorption are followed by a rate determining step in which OH and glyoxal molecules react with each other. At higher pH values the oxide coverage starts to interfere, giving rise to a modification in the reaction path.

1. Introduction

There have been many studies of the electrocatalytic activity of noble metals with respect to the oxidation of organic substances. This is because of the potential of organic substances for use as fuels in electrochemical energy converters [1]. Further, the search for electrochemical means of enhancing the rates and yields in specific products of economic importance using organic reactions also constitutes an important reason for the interest in these studies.

Gold has been reported to be a good electrode material for the synthesis of some organic compounds. The oxidation rate of many organic substances on gold electrodes, however, is usually lower than it is on platinum. This is especially valid for the oxidation of saturated organic molecules in acidic medium. On Pt, the oxidation of such substances is facilitated by its previous dissociative adsorption, as in the case of aliphatic alcohols [2]. This kind of adsorption does not take place on Au electrodes in acidic medium, so that only very low oxidation currents can be detected [3]. The coverage of the gold electrode with OH in an alkaline medium provides a

0378-7753/89/$3.50

new reaction path, since the OH radicals can react with H atoms of the substance in solution or adsorbed, and the oxidation currents can become rather high [4].

Unlike aliphatic compounds, unsaturated organic molecules can be adsorbed onto gold surfaces in acidic medium [5] and can oxidize on those electrodes. The adsorption of unsaturated compounds on bare gold surfaces seems to proceed through interaction between the π^* antibonding orbitals of the organic molecule and the filled d-electron levels on surface sites in polycrystalline gold [5].

We present below a study of the mechanism of electro-oxidation of glyoxal on gold polycrystalline electrodes in acidic medium. This oxidation takes place after adsorption of glyoxal molecules, which takes place because a π^* antibonding orbital is also present in glyoxal. The study allowed the determination of reaction orders, Tafel slopes, apparent activation energy and entropy and, by using diagnostic criteria, it was possible to establish coherent reaction mechanisms. These experimental data were interpreted using two different mechanisms, valid for low pH values and higher pH values (up to about pH = 2.7) in which OH and oxide coverage, respectively, played an important role.

2. Experimental

A three-compartment electrochemical cell was used in this study with a 1 cm^2 rectangular plate of polycrystalline gold (99.99%-pure) working electrode. The counter electrode was a 0.5 mm dia. gold wire rolled up to form a spiral. The cell compartments were separated by sintered G-3 glass frits, and a Luggin capillary placed 1 mm from the working electrode surface minimised the resistance of the electrolyte. As a reference electrode $Hg/Hg_2SO_4/K_2SO_4/(MSE)$ was used in the same solution.

The solutions were prepared from AnalaR grade chemicals (Merck) and water which had been distilled and doubly deionized by means of a Millipore system (Mod. Milli Q.). The temperature was either maintained at 25.0 ± 0.10 °C, or varied for the measurement of the apparent activation enthalpy.

The solutions were agitated by means of a nitrogen flow and the experiments were carried out under an inert nitrogen atmosphere. Before each experiment, the working electrode was activated by applying repetitive triangular potentiodynamic scans at 200 mV s^{-1} between the potential limits corresponding to oxygen and hydrogen evolution, until a stationary voltammogram was obtained.

3. Results

3.1. General aspects of the electrochemical behaviour of glyoxal on gold

Figure 1 shows a typical cyclic voltammogram recorded at a sweep rate of 200 mV s^{-1} for gold in a 0.5 M H_2SO_4 acidic solution. The addition of

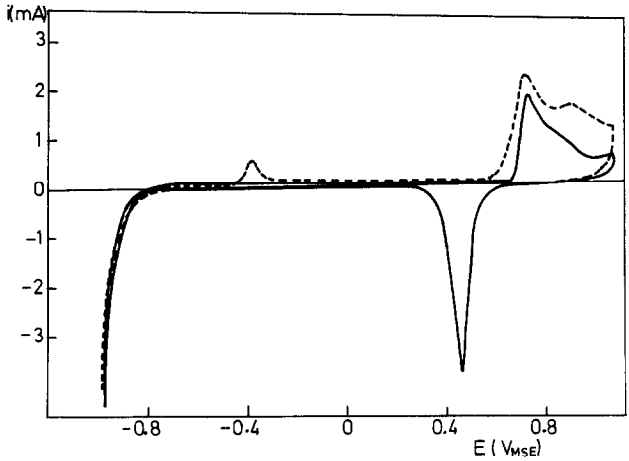

Fig. 1. Cyclic voltammogram of a gold electrode in acidic medium (0.5 M H_2SO_4, 25 °C, $v = 200$ mV s^{-1}); — — —, cyclic voltammogram for a gold electrode in acidic medium in the presence of 5×10^{-2} M glyoxal under the same conditions.

5×10^{-2} M glyoxal produces a change in the voltammetric i–E curve. When the potential scan starts at potential values at which H_2 is evolved on the gold electrode, a first current peak is now observed at -0.4 V_{MSE}. Two more oxidation peaks appear in the potential range between $+0.7$ and $+0.9$ V_{MSE} corresponding to the electro-oxidation of glyoxal. The current–potential curve starts to rise at potentials approximately 100 mV more negative than the potential range at which gold oxides are formed (Fig. 1). In the case in which the peak in the double layer region (at -0.4 V_{MSE}) appears, an enhancement of the double layer current is observed, as well as an increase in the currents attributed to glyoxal oxidation.

A change in the sweep rate gives rise to an increase in the oxidation current, as can be seen in Fig. 2(a). Figure 2(b) shows a plot of the oxidation current density, i_p *versus* $v^{1/2}$. At low sweep rates the curve is similar to that worked out by Wopschall and Shain [6] and was interpreted as typical behaviour for the oxidation of a weakly adsorbed substance. Furthermore, with potential scans carried out at slow sweep rates, no second oxidation peak is detected. A second oxidation peak appears from a sweep rate of 50 mV s^{-1}.

Increasing the lower scan limit causes the double layer peak to disappear but scarcely influences the oxidation peak of glyoxal.

Such oxidation peaks are not observed when studying the oxidation of formaldehyde, or acetaldehyde on gold in acidic medium.

3.2. Influence of glyoxal concentration

Figure 3 gives the variation of i_p as a function of glyoxal concentration, C_G. The curve obtained presents the form of an adsorption isotherm, confirming the need of an adsorption step of glyoxal previous to its oxidation.

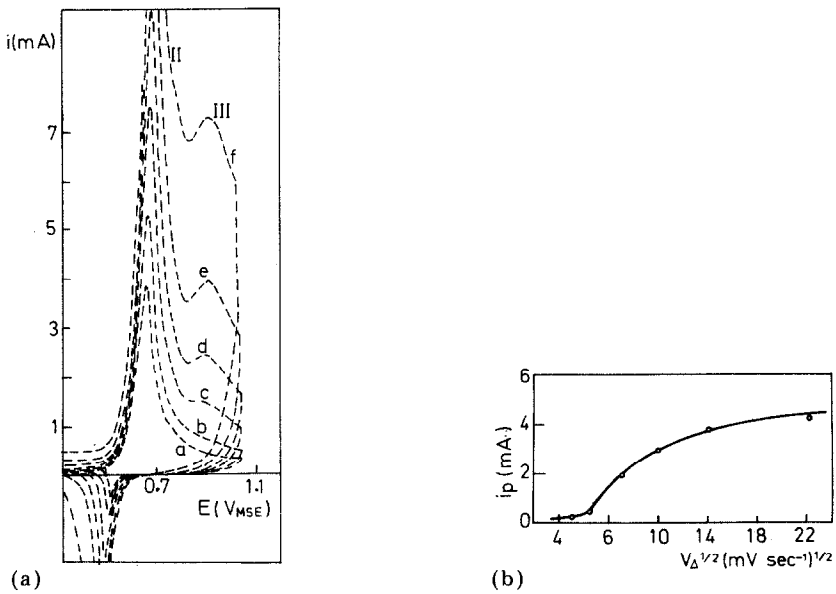

Fig. 2. (a) Influence of the sweep rate on the oxidation currents for glyoxal (0.5 M H_2SO_4 + 5 × 10^{-2} M glyoxal, T = 40 °C). Curves a, b, c, d, e, f correspond to the following sweep rates: a = 10, b = 20, c = 50, d = 100, e = 200, f = 500 mV s^{-1}. Cathodic scan limit = −0.95 V_{MSE}. (b) Plot of i_p for the peak at less positive potentials *vs.* $v^{1/2}$.

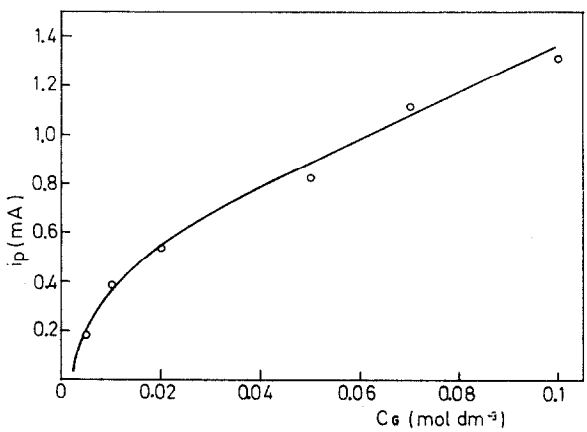

Fig. 3. Plot of i_p *vs.* glyoxal concentration in solution. The same conditions as before. T = 25 °C, v = 5 mV s^{-1}.

On the other hand, in Fig. 4 values of log i (i in mA) *versus* the logarithm of glyoxal concentration are plotted at different potential values (T = 25 °C). The values were taken from quasistationary measurements at v = 5 mV s^{-1} in a 0.5 M H_2SO_4 solution). The deduced value for the reaction order with respect to glyoxal concentration is $Z_G \simeq 0.75$, and does not change with the potential value.

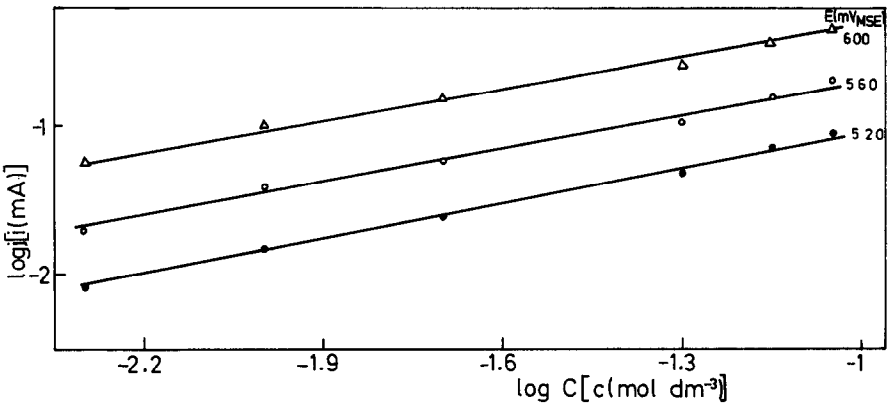

Fig. 4. Plots of log i *vs.* the logarithm of glyoxal concentration at different potentials, 0.5 M H_2SO_4, T = 25 °C and v = 5 mV s^{-1}. Z_G = 0.75.

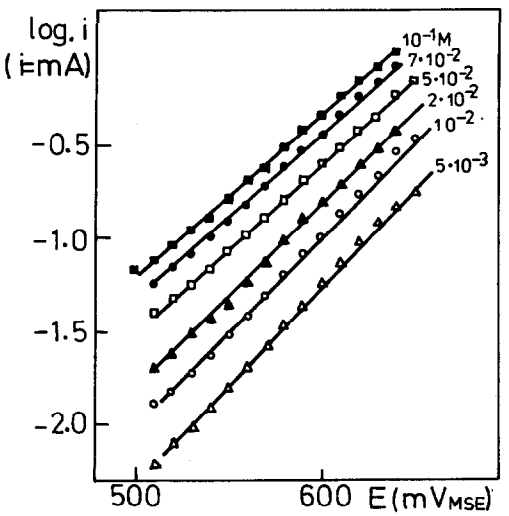

Fig. 5. Modification of the Tafel slope values with different glyoxal concentrations. 0.5 M H_2SO_4, v = 5 mV s^{-1}. T = 25 °C.

Figure 5 shows the plot of a series of Tafel slopes obtained in the same potential range by changing the glyoxal concentration. These values were measured from linear voltammograms recorded at v = 5 mV s^{-1} (*i.e.*, under quasistationary conditions) in 0.5 M H_2SO_4 and changing the glyoxal concentration from 5×10^{-3} to 10^{-1} M. There is a slight increase in the Tafel slope value with increasing glyoxal concentration from 94 to 112 mV.

3.3. Influence of the pH value

There is a linear decrease in the potential at half peak height ($E_{p1/2}$) and an almost exponential decrease of i_p with pH for the oxidation peak of glyoxal, as illustrated in Fig. 6(a) and (b), respectively.

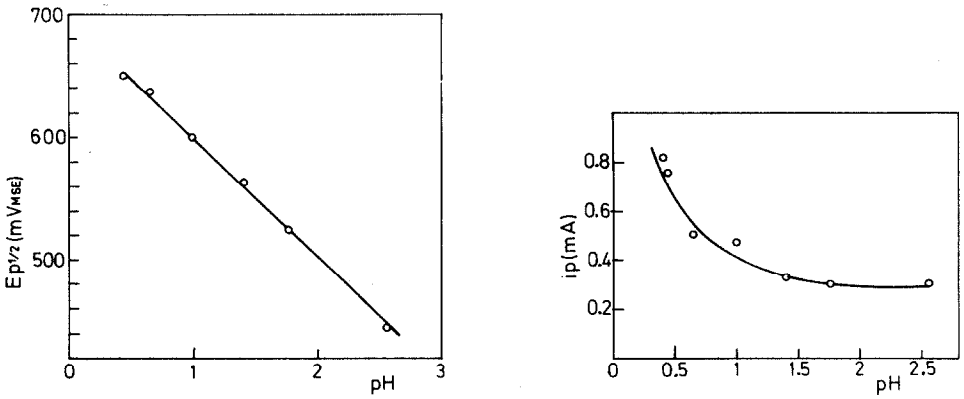

Fig. 6. Plots of $E_{p1/2}$ *vs.* pH (slope = 97 mV) (a), and of i_p *vs.* pH (b), 5×10^{-2} M glyoxal. T = 25 °C, v = 5 mV s^{-1}, for the first current peak in Fig. 2(a).

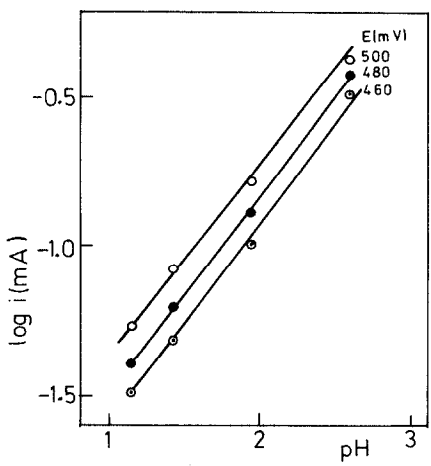

Fig. 7. Determination of the reaction order with respect to H^+ concentration in solution at different potential values. 5×10^{-2} M glyoxal. T = 25 °C, v = 5 mV s^{-1}, $Z_{H^+} = -0.67$.

Figure 7 shows plots of log i *versus* pH value for three different potential values. The pH was varied by changing the H_2SO_4 concentration and adjusting the ionic strength to a constant value by adding K_2SO_4. The resulting reaction order with respect to proton concentration is −0.67, and remains unmodified when changing the potential value.

Figure 8 shows a series of Tafel slopes obtained for 5×10^{-2} M glyoxal concentration for various pH values. The variation in the Tafel slope with pH is summarized in Table 1. It can be seen that a very rapid increase in the Tafel slope takes place when the pH is increased.

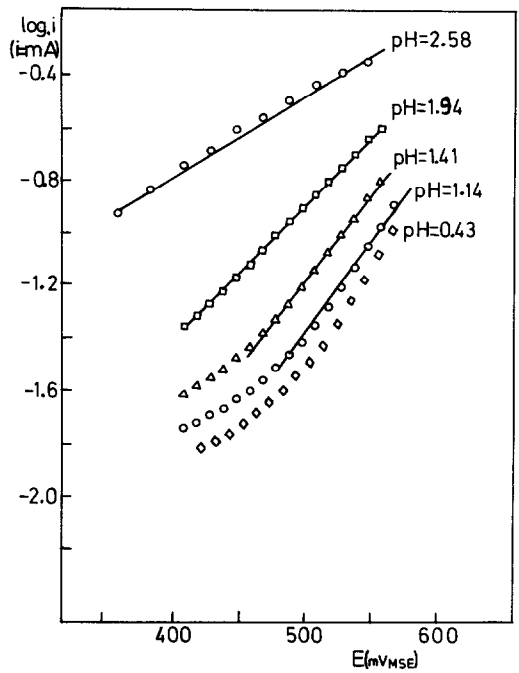

Fig. 8. Tafel slopes determined at different pH values: 5×10^{-2} M glyoxal, T = 25 °C, v = 5 mV s^{-1}.

TABLE 1

Variation of the Tafel slope (b) with the pH value. T = 25 °C, $C_{glyoxal} = 5 \times 10^{-2}$ M

pH	b (mV current decade^{-1})
0.3 - 0.4	94
1.14	120
1.41	120
1.94	194
2.58	304

3.4. Effect of temperature variation on glyoxal oxidation

Figure 9 shows plots of log i *versus* $1/T$ (K^{-1}) at different potential values. The currents at a given potential increase with increasing temperature. The plots of log i *versus* $1/T$ are linear and, from their slopes and intercepts, values of the apparent activation enthalpy and entropy can be deduced, which are summarized in Table 2.

The high value of the apparent activation enthalpy obtained, and its independence of pH, are in agreement with a chemical rate determining step in which no protons are involved.

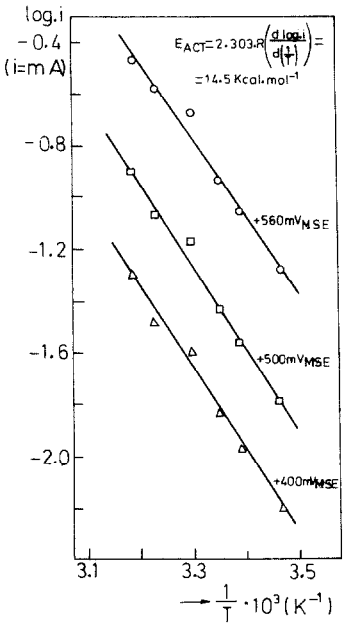

Fig. 9. Dependence between log i and T^{-1} (K^{-1}) at different potential values. 0.5 M H_2SO_4 + 5 × 10^{-2} M glyoxal. v = 5 mV s^{-1}.

TABLE 2

Values of the apparent activation enthalpy (ΔH^*) and entropy (ΔS^*) measured at different potential values.
System: gold + 0.5 M H_2SO_4 + 5 × 10^{-2} M glyoxal

E (mV_{MSE})	ΔH^* (kJ mol^{-1})	ΔS^* (J mol^{-1} K^{-1})
400	57.6	158
500	59.8	173
560	53.6	162

Other observations made during the temperature variation study were:

(i) at 15 °C and v = 5 mV s^{-1} in a 0.5 M H_2SO_4 + 5 × 10^{-2} M glyoxal solution, two oxidation peaks of glyoxal were detected. An increase in the temperature gives rise to an increase in the current corresponding to the first peak, whereas the current corresponding to the second peak gradually diminishes to a limiting value at $T \simeq 40$ °C;

(ii) the temperature increase gives rise to the appearance of a new peak during the negative scan. This is situated in the potential range close to that at which the first peak appeared and grows with increasing temperature.

4. Discussion

4.1. Reaction mechanism at pH ⩽ 0.5

Since i_p varies with glyoxal concentration (Fig. 3) (as in the case of an adsorption isotherm), the oxidation of glyoxal on gold, in the potential range at which the formation of gold oxide starts, must take place via the adsorption of glyoxal on the electrode surface. Further, the plot of i_p *versus* $v^{1/2}$ (Fig. 2(b)) seems to confirm the requirement [6] of a weak adsorption of the reactant previous to its oxidation. The oxidation reaction at pH ⩽ 0.5 also requires the presence of OH coverage, since it begins at potential values close to that of gold oxide formation. The values of the reaction orders with respect to glyoxal and proton concentrations are fractional, and this indicates that glyoxal and OH adsorption play a role [1]. The apparent activation enthalpy is about 57 kJ mol^{-1}, a rather high value, in agreement with a rate determining step (RDS) in which chemical bonds are broken. The invariance of ΔH^* with potential indicates an RDS chemical in nature without charge transfer. Also, the positive value of the apparent activation entropy indicates an activated complex more disordered than the reactants. This can be true, since one of the postulated reactants is the OH coverage, in which the linkage through hydrogen bonds between the OH radicals can be considered as an ordered state [7] which is distorted by the reaction with contiguous glyoxal adsorbed molecules.

Summarizing, the theoretical mechanism proposed for the oxidation of glyoxal on gold at pH ⩽ 0.5 must account for the following experimental rate equation:

$$i = k\, C_G^{3/4}\, C_{H^+}^{2/3} \exp\left[\frac{\bar{\alpha}\, FE}{RT}\right]$$

where $\bar{\alpha}$ = a transfer coefficient ≃ 2/3, and must be in agreement with the other experimental facts observed.

On the basis of the points discussed above , the following reaction mechanism for the oxidation of glyoxal on polycrystalline gold at pH ⩽ 0.5 is proposed:

Step 1 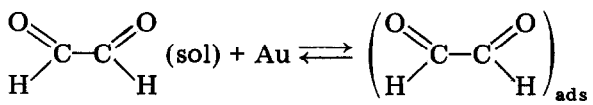 (sol) + Au ⇌

Step 2 $Au + HOH \rightleftharpoons Au\text{–}OH + H^+ + e^-$

Step 3 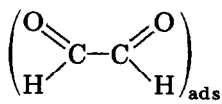 + Au–OH ⟶ 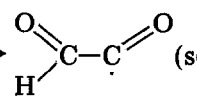 (sol) + Au + HOH

(rate determining step)

Only these first three steps will be taken into account for the deduction of the theoretical rate equation although the following steps are postulated to give the known end products: glyoxolic acid and CO_2.

Step 4 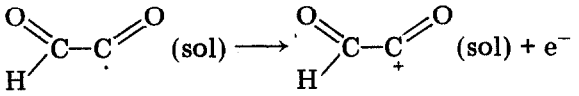 (sol) + e^-

Step 5 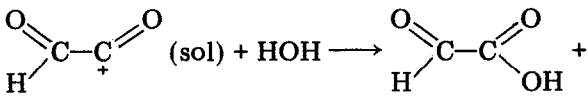 (sol) + HOH + H^+

Step 6 Au—OH + 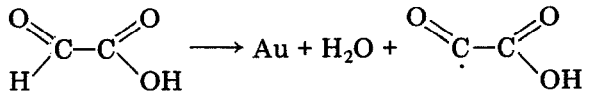 Au + H_2O +

Step 7 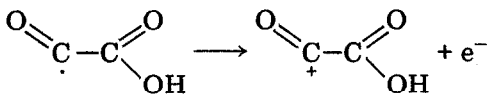 + e^-

Step 8 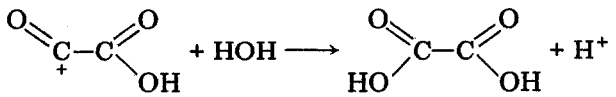 + HOH + H^+

and finally:

$$COOH\text{–}COOH \longrightarrow 2CO_2 + 2H^+ + 2e^-$$

in subsequent steps.

From the rate determining step the following rate equation can be derived:

$$i = nFv_3 = nFk_3\theta_{OH}\theta_G \exp\left[(1-\gamma_G)\frac{f(\theta)}{RT}\right] \cdot \exp\left[(1-\gamma_{OH})\frac{f(\theta)}{RT}\right] \qquad (1)$$

where θ_{OH} and θ_G represent the surface coverages with OH and glyoxal, respectively. The exponential terms indicate that step 3 takes place with a desorption of glyoxal and OH coverages. $f(\theta)$ represents an interaction coefficient which is a function of the total coverage (with OH, glyoxal, and oxide), and γ_G and γ_{OH} are two symmetry coefficients for the adsorption of glyoxal and OH under Temkin conditions [8]. Step 3 in the proposed mechanism is accomplished after the breaking of an Au—OH and C—H bond, which explains the high value found for the apparent activation enthalpy.

It has been supposed that OH and glyoxal adsorption satisfy a Temkin isotherm, *i.e.*, the θ_{OH} and θ_G values must range between 0.2 and 0.8. Thus, by considering steps 1 and 2 in quasiequilibrium, the following equations can be deduced:

$$\exp\left[\frac{f(\theta)}{RT}\right] \simeq K_1 C_G \qquad (2)$$

$$\exp\left[\frac{f(\theta)}{RT}\right] \simeq K_2 C_H^{-\frac{1}{4}} \exp\left[\frac{FE}{RT}\right] \qquad (3)$$

where K_1 and K_2 represent equilibrium constants for steps 1 and 2 and C_G the glyoxal concentration in the bulk of the electrolyte.

Raising both terms in eqn. (2) to the power $(1-\gamma_G)$, and both terms in eqn. (3) to the power $(1-\gamma_{OH})$, and substituting the resulting eqns. in eqn. (1), the following expression for the theoretical rate equation is obtained:

$$i = nF\,K\,C_{H^+}^{-(1-\gamma OH)}\,C_G^{(1-\gamma G)}\exp\left[(1-\gamma_{OH})\,\frac{FE}{RT}\right] \tag{4}$$

where $K = k_3\theta_G\theta_{OH}K_2^{(1-\gamma OH)}K_1^{(1-\gamma G)}$

This expression coincides with the experimental rate equation when $\gamma_{OH} = 1/3$ and $\gamma_G = 1/4$. In that case the theoretical values for $Z_{H^+} = -0.66$, $Z_G = 3/4$ and $b = 94$ mV (current decade)$^{-1}$, in complete agreement with the kinetic parameters determined in the experiments.

4.2. Reaction mechanism at $0.5 \leqslant pH \leqslant 2.6$

As previously described, increasing the pH produces a rapid increase in the Tafel slope (Fig. 8 and Table 1) and a decrease in i_p, whereas the current increases at potentials more negative than E_p. The last effect of increasing pH could be the consequence of an easier OH coverage formation. This starts at more negative potentials, resulting in a higher OH coverage which, initially, would have a positive effect on the rate determining step. The decrease of i_p with pH indicates that the higher OH coverage can facilitate gold oxide formation. This interferes with the glyoxal oxidation in two ways:

(a) when θ_O grows, there is less room for glyoxal adsorption so that $\theta_G \to 0$, and this adsorption can be supposed to occur, satisfying a Langmuir isotherm;

(b) the oxide coverage interacts with glyoxal molecules, producing a chemical oxidation in which the rate increases rapidly with temperature, thus explaining the limiting current observed at 40 °C in the most positive potential range. This interaction can be expressed as follows:

$$Au_xO_y + \text{Glyoxal} \longrightarrow x\,Au + \text{Oxidation products}$$

At 40 °C the diffusion of glyoxal molecules in the electrolyte could be responsible for the limiting current obtained. At lower temperatures and growing sweep rates a second current peak is observed, probably due to the oxidation of an intermediate formed at less positive potentials (first oxidation peak).

The effect of the higher pH and the increasing gold oxide layer are more accentuated on the Tafel slope values (Table 1) and on the Z_{H^+} value which gradually changes from $-2/3$ to $-1/2$, and the Z_G value which tends to 1.

Thus, at $pH \geqslant 0.5$, a new experimental rate equation can be written:

$$i = nFk'C_G\,C_{H^+}^{-x}\exp\left[\frac{xFE}{RT}\right] \tag{5}$$

where x can take values from 0.5 to 0.2 with decreasing pH values.

The following new reaction mechanism is proposed:

Step 1 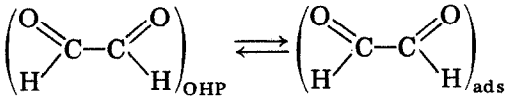

Step 2 $Au + HOH \rightleftharpoons AuOH + H^+ + 1e^-$

Step 3 $x\,AuOH \rightleftharpoons Au_xO_y + x/2H_2O$ where $y = x/2$

Step 4 $G_{ads} + Au_xO_y \longrightarrow H_2O +$ 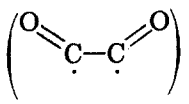

Step 5 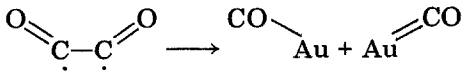

Step 6 $Au{-}CO + Au_xO_y \longrightarrow Au_xO_{y-1} + Au + CO_2$

From the rate determining step, the rate equation should be:

$$i_4 = nFk_4\theta_G\theta_O \tag{6}$$

where the absence of exponential terms indicates that a Langmuirian desorption of OH and glyoxal have been supposed. This can be explained, since an increase in pH makes $\theta_{OH} \geqslant 0.8$, so that:

$$\theta_{OH} \simeq K_2 C_{H^+}^{-1} \exp\left[\frac{FE}{RT}\right] \tag{7}$$

and

$$\theta_G \simeq K_3 C_G \tag{8}$$

for the very low glyoxal coverages allowed by the high θ_{OH} and θ_O coverages.

From step 3 in quasi-equilibrium the following equation is obtained either when interaction (Temkin behaviour) occurs, or when no interaction in the oxide coverage (Langmuir behaviour) is assumed:

$$\theta_O = K_2\theta_{OH}^x \tag{9}$$

It is derived by equating the following forward and back rate equations for this step:

$$v_3 = k_3\theta_{OH}^x \exp\left[\frac{(1-\gamma_{OH})f(\theta_T)}{RT}\right] \exp\left[-\gamma_O \frac{f(\theta_T)}{RT}\right] =$$

$$v_{-3} = k_{-3}\theta_O \exp\left[(1-\gamma_O)\frac{f(\theta_T)}{RT}\right] \exp\left[-\gamma_{OH}\frac{f(\theta_T)}{RT}\right]$$

Therefore, a substitution of eqns. (7) - (9) in eqn. (6) leads to the expression:

$$i = nFK' C_{H^+}^{\bar{x}} C_G \exp\left[\frac{xFE}{RT}\right] \quad (10)$$

which is identical to the experimental rate equation (5) and explains the experimental values of the Tafel slope and reaction orders obtained at pH = 1.14 and 1.41 (for $x = 0.5$), pH = 1.94 (for $x = 0.3$) and pH = 2.58 (for $x = 0.2$).

5. Conclusions

Unlike other saturated aldehydes and alcohols, glyoxal oxidizes on polycrystalline gold electrodes in acidic medium. The reason for this different behaviour is postulated to be the adsorption of glyoxal molecules on gold electrodes due to the possibility of adopting a planar shape with a π^* antibonding region able to overlap with filled d orbitals on gold surface sites.

Either surface OH or oxide groups take part in the oxidation mechanism, depending on the solution pH. In both cases, mechanisms for glyoxal oxidation were advanced which are consistent with the experimental observations.

Acknowledgements

Support of this research by the D.G.I.C. y T. (Grant No.P.B.86-0565) is gratefully acknowledged.

The author thanks R. Contonente and R. Celdrán for their contributions to the experimental work.

List of symbols

$\bar{\alpha}$	Anodic transfer coefficient
γ_G	Symmetry coefficient for activated adsorption of glyoxal on gold
γ_{OH}	Symmetry coefficient for activated adsorption of OH on gold
θ_G	Surface coverage with glyoxal
θ_{OH}	Surface coverage with OH
ΔH^*	Activation enthalpy for the reaction mechanism studied (kJ mol^{-1})
ΔS^*	Activation entropy for the reaction mechanism studied (J mol^{-1} K^{-1})
b	Tafel slope (mV (current decade)$^{-1}$)
C_G	Concentration of glyoxal in the electrolyte (mol dm^{-3})
C_{H^+}	Concentration of H_3O^+ in the electrolyte (mol dm^{-3})
E	Potential value measured *vs.* MSE (V or mV)

F	Faraday constant (964 867 × 10^4 C mol^{-1})
i	Anodic current = reaction rate (mA)
i_p	Peak current (mA)
k	Chemical rate constant = rate constant at $E = 0$
MSE	Mercury sulphate reference electrode
rds	Rate determining step
R	Gas constant (831 434 J mol^{-1} K^{-1})
T	Temperature (K or °C)
v	Potential sweep rate (mV s^{-1})
Z_G	Reaction order with respect to glyoxal concentration
Z_{H^+}	Reaction order with respect to pH

References

1 J. O'M. Bockris and S. Srinivasan, *Fuel Cells*, McGraw-Hill, New York, 1969.
2 E. Sokolova, *Electrochim. Acta*, *20* (1975) 323; *24* (1979) 147.
3 M. W. Breiter, *Electrochim. Acta*, *8* (1963) 973.
4 M. Beltowska-Brzezinska and W. Vielstich, *Electrochim. Acta*, *22* (1977) 1313; *24* (1979) 407.
5 R. Celdrán and J. González-Velasco, *Electrochim. Acta*, *26* (1981) 763.
6 R. H. Wopschall and I. Shain, *Anal. Chem.*, *39* (1967) 1514.
7 C. Alonso and J. González-Velasco, *Z. Phys. Chem. (Leipzig)*, *269* (1968) 65.
8 See: E. Gileadi and B. E. Conway (eds.), *Modern Aspects of Electrochemistry*, Vol. III, Butterworths, London, 1964, Ch. 5.